



Pulse to pulse control for highly precise and efficient micromachining with femtosecond lasers

G. MINCUZZI,^{1,*} E. AUDOUARD,² A. BOURTEREAU,¹ M. DELAIGUE,² M. FAUCON,¹ C. HOENNINGER,² K. MISHCHIK,² A. REBIÈRE,¹ S. SAILER,³ A. SEWERYN-SCHNUR,³ AND R. KLING¹ 

¹ALPhANOV, Technological Centre for Optics and Lasers, Optic Institute of Aquitaine, Rue F. Mitterrand 33400 Talence, France

²AMPLITUDE, 11 Avenue de Canteranne, Cité de la Photonique, 33600 Pessac, France

³SCANLAB GmbH, Siemensstrasse 2a, 82178 Puchheim Munich, Germany

*girolamo.mincuzzi@alphanov.com

Abstract: Micromachining with high repetition rate femtosecond lasers and galvo scanners shows some limitations in the pulses positioning accuracy due to the galvo mirrors acceleration. This is particularly evident during scan speed or direction changes, resulting in a poor quality and overtreatment e.g. in corners. Several scanning approaches have been proposed to tackle these issues like the so-called skywriting (SW) and the pulse-on-demand (POD) being the last limited to ns lasers, moderate pulse repetition rates and scan speeds. Recently, POD approach has been extended to femtosecond laser sources with high power and high repetition rate. Here, for the first time, we explored the huge potential in laser micromachining of femtosecond POD technology associated to a fast galvo scanner. We tested an innovative set-up allowing for precise laser triggering at the requested time and position for MHz repetition rate and scan speed as high as 20 m/s. The pulse position accuracy of the system has been estimated to be $\leq 1\mu\text{m}$ whilst performances have been evaluated in comparison to conventional scanning and SW. Finally, we report the results of an engraving test on stainless steel. The advantages of the approach we propose are clearly shown in terms of machining quality and precision with respect to conventional scanning and reduction of the processing time by $\approx 40\%$ with respect to SW.

© 2020 Optical Society of America under the terms of the [OSA Open Access Publishing Agreement](#)

1. Introduction

The use of ultrashort pulse lasers (UPLs) in micromachining provides numerous advantages, such as the ability to enable new fabrication processes which cannot be accomplished with longer pulses [1–3]. Additionally, UPLs achieve the highest machining precision and quality in applications like cutting, drilling, engraving, milling, etc. [4–7]. Features such as these have driven a remarkable increase of UPL technological readiness in recent years. Rugged, reliable, high power, industrial UPLs are now available on the market, delivering an average power P of several hundreds of Watts with repetition rates reaching several MHz [8–14]. At these powers, unwanted heat accumulation phenomena can arise due to excessive pulse overlapping thus limiting the full exploitation of the laser performance [15–17]. To mitigate or even prevent this risk, innovative optomechanical systems have been developed and placed on the market enabling scan speeds well beyond tens of meters per second in both modes vectorial scanning (2D) [18] and raster scanning (1D) [19]. Following this technological approach we have recently shown that it is possible to effectively texture metallic surfaces with a repetition rate of 10 MHz and scan speed of 200 m/s, and also cut micro-mechanical components with a repetition rate of 1 MHz and scan speed of 2 m/s [20,21]. Nonetheless, deficiencies in the synchronization of the positioning of beam deflection device and laser triggering, still lead to machining defects. We mention

for instance overtreatment due to the inertia of the mirrors of galvanometer scanners or path deviations at complex shapes. In the case of polygon scanner heads, techniques of highly precise pulses triggering have been introduced enabling an increase of the pulse positioning accuracy to few μm [22]. This is also true for scan speed values as high as several tens of m/s. In the case of galvo scanners, pulse overlapping tends to be modified when the laser path entails acceleration. This can cause issues for applications such as engraving, where an excessive material ablation can be observed in the pattern edges, or scribing of geometric paths including sharp corners, which tend to either be rounded or overtreated. In this case, a possible approach is SW, in which the laser is switched-off during acceleration and a supplementary mirror movement is made to accomplish the variation. Once this is completed, pulses are delivered again. This technique entails an extra time which can induce a throughput reduction in the case of complex patterns and multiple direction changes. This issue is overcome with the so-called pulse-on-demand (POD) technique [23]. In this case the opto-mechanical system positioning the pulses (for example a galvo scanner) can predict the exact time to trigger the pulse emission to ensure the desired location of the laser pulses. Techniques such as switch gain and Q-switch, make it possible to modify the laser repetition rate and adapt it in order to promptly trigger the pulse emission [24,25]. However, these architectures are limited to pulse widths in the nanosecond domain and pulse repetition rates below 1 MHz (typical even lower, tens to hundred kHz). This still causes a lack of precision, especially at scan speed as high as 20 m/s. Here a novel technological approach is proposed and tested making possible the POD also for femtosecond laser and dramatically increasing the positioning precision in time and in space. The Spot Distance Control feature of the galvo scanner controller (RTC) allows one to calculate and predict the actual beam position also including mirrors acceleration and/or deceleration. An UPL, based on a mode-locked master oscillator and a power amplifier in chirped pulse amplification (CPA), having the pulse on demand feature FemtoTrig has been recently developed and here utilized for the first time [26,27]. FemtoTrig ensures pulses at constant energy and negligible timing jitter at any user trigger interval. User trigger intervals may vary from seconds down to a few periods of the mode-locked oscillator's pulse period $T_{\text{osc}} = 1/f_{\text{osc}}$, f_{osc} being the oscillator pulse repetition rate which is typically in the range of some 10 MHz. The constant pulse energy is achieved by precise control of the laser gain through the amplifier chain. The timing jitter is as low as one period of the mode-locked master oscillator: $T_{\text{jitter}} = 1/f_{\text{osc}}$. According to the precise position feedback, a controller will dynamically adjust the pulse to pulse delay and accomplish constant energy deposition at any programmed scan pattern and trajectory. We have combined these two recent innovations in a single set-up (hereinafter called POD-FT) to validate the synchronization and constant pulse separation at various scan speeds and geometrical patterns and demonstrate the huge potential of this combination for high throughput and high precision laser machining. Applications trials like engraving with scan speed up to 20 m/s are presented in comparison to conventional scanning approach and SW to demonstrate the benefit of the fast synchronization and pulse on demand technologies also for femtosecond lasers.

2. Experimental

We carried out four different tests (i), (ii), (iii) and (iv). In all the four tests we used a CPA, UPL emitting in the IR ($\lambda = 1030$ nm) and converted by THG to UV, $\lambda = 343$ nm (Tangor, provided by Amplitude Système). The maximum P it could deliver at this wavelength was $P = 32$ W. The pulse duration was 350 fs. Thanks to the FemtoTrig method the user can select the pulses he needs from the oscillator train conserving the same energy per pulse or burst of pulses. The latency delay between the trigger signal (sent to the controller by the scanner) and the emergence of the pulse at the output of the laser was constant. The uncertainty on this delay is lower than 25 ns i.e. one oscillator period. The nominal optimal configuration i.e. nominal repetition rate and nominal number of pulses in a burst is factory set. P is maximum for this configuration.

Furthermore, the energy per pulse and the number of pulses in the burst will be kept constant for all repetition rate values lower than the nominal one. Thanks to this feature the ablation is kept unchanged during slow down and acceleration phases of the scanner. During all the tests, the beam was coupled into a galvo scanner excelliSCAN 14 and driven by a RTC6 board, both provided by SCANLAB, and then focused through an f-theta lens with focal length $f = 100$ mm (spot size $2\omega_0 = 15$ μm). The scanner board was controlled by two different control software.

To test the set-up reliability (test (i)) the software control (DMC provided by Direct Machining Control) was programmed to scan a line of 10 mm with different scan speed values $v = 10$ m/s, $v = 15$ m/s, $v = 20$ m/s at a constant repetition rate $f = 1$ kHz. The corresponding TTL signal generated from the RTC6 was used to gate a function generator (Tombak by Aerodiode). The Tombak was programmed to emit a sequence of pulses with a varying temporal distance Δt . In particular, for each v value, we fixed two sets of Δt enabling the first a pulse-to-pulse distance $d = 20$ μm , $d = 21$ μm , $d = 22$ μm , $d = 23$ μm , $d = 24$ μm , $d = 25$ μm , and the second $d = 10$ μm , $d = 20$ μm , $d = 30$ μm , $d = 40$ μm . In test (ii) we compared POD-FT performances with conventional scanning and SW. In this case the control software (laserDESK provided by SCANLAB) was programmed to scan squares of 5 cm \times 5 cm using the three previously mentioned approaches (see Fig. 1 part 1 plus part 2). In the conventional approach we fixed a set of values of repetition rate f and v corresponding to $d = 25$ μm , namely $f = 100$ kHz / $v = 2.5$ m/s, $f = 400$ kHz / $v = 10$ m/s, $f = 600$ kHz / $v = 15$ m/s, $f = 800$ kHz / $v = 20$ m/s. Identically, in the SW approach (automatically managed via LaserDESK) the same f/v values were used. Finally, in the POD-FT approach we fixed $d = 25$ μm and varied v ($v = 2.5$ m/s, $v = 10$ m/s, $v = 15$ m/s and $v = 20$ m/s).

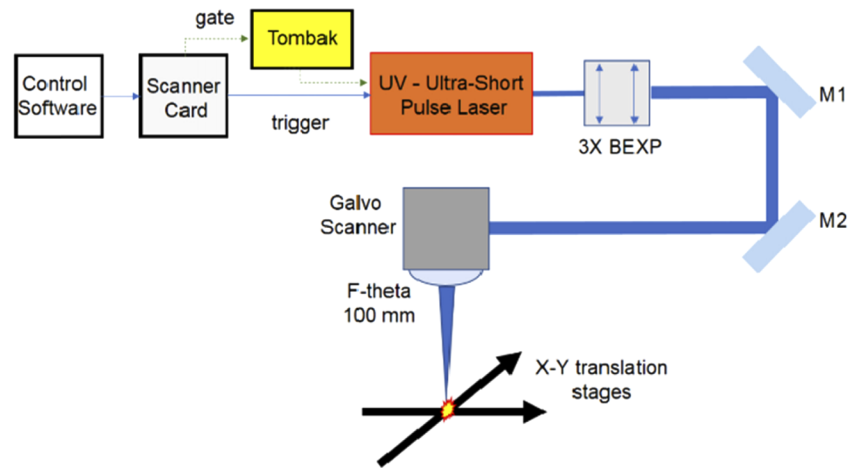


Fig. 1. The figure shows a schematic of the experimental apparatus.

In test (iii) we carried out engraving tests to further compare the mentioned scanning approaches: conventional scanning, SW and POD-FT. We used the same set-up as in test (ii). For conventional scanning and SW we varied v ($v = 0.9$ m/s, $v = 3.6$ m/s, $v = 7.2$ m/s) and proportionally f ($f = 100$ kHz, $f = 400$ kHz, $f = 800$ kHz) in order to keep $d = 9$ μm as well as the pulse overlapping (40%) unchanged. For the POD-FT we fixed $d = 9$ μm and we varied v ($v = 0.9$ μm , $v = 3.6$ μm and $v = 7.2$ μm). In all cases we engraved a letter “A” (size ≈ 3 mm \times 3 mm) with 75 scan repetitions and a hatch of 3 μm . The scanning direction between two successive scans was varied with a fix increment of 14.4° . Results were analysed via optic microscope (MF-A1010H provided by Mitutoyo), profilometer (DCM3D provided by Leica) and SEM (Vega provided by Tescan). Test (iv) was the same as (ii), except that it was carried out with a different control software

(DMC + XL SCAN). The last one makes possible to compensate the above-mentioned latency delay. Tests (i) was carried out on PET whilst tests (ii), (iii) and (iv) were carried out on polished stainless steel with a pulse energy $E = 4 \mu\text{J}$. Squares relates to test (ii) were marked 10 times.

3. Results and discussion

3.1. Set-up reliability

Figure 2 left, shows the visual appearance of laser pulses impacts triggered with POD-FT when $v = 10 \text{ m/s}$, $v = 15 \text{ m/s}$ and $v = 20 \text{ m/s}$. The trigger signal consists of a sequence of electronic pulses having a variable temporal delay Δt . The last is adjusted to enable a relative distance between two successive impacts δ varying from $\delta = 20 \mu\text{m}$ to $\delta = 25 \mu\text{m}$ with a step of $1 \mu\text{m}$. To evaluate the reliability of the POD-FT, δ was measured via software (Gwiddion) and plotted in Fig. 2 right. As visual reference the ideal case relative to a set of impacts in which the pulse distance is exactly $1 \mu\text{m}$ is also plotted (dashed black line). From the linear fit of the measurements (red circles for $v = 10 \text{ m/s}$, green triangles for $v = 15 \text{ m/s}$ and black squares for $v = 20 \text{ m/s}$) the values of slopes η for each v was extracted. The last corresponds to the average increment of δ when passing from one impact to the next one. For the reference case $\eta = 1 \mu\text{m}/\text{impact}$. From our measurements we obtained $\eta = 1.02 \pm 0.05 \mu\text{m}/\text{impact}$, $\eta = 0.98 \pm 0.04 \mu\text{m}/\text{impact}$ and $\eta = 1.00 \pm 0.05 \mu\text{m}/\text{impact}$ for $v = 10 \text{ m/s}$, $v = 15 \text{ m/s}$ and $v = 20 \text{ m/s}$, respectively. Furthermore, excluding the case of $v = 15 \text{ m/s}$ and $\# = 5$, the discrepancy between the reference and all our measurements is lower than the uncertainty induced by the jitter $\Delta\delta$ ($\Delta\delta = 0.5 \mu\text{m}$ black line, $\Delta\delta = 0.375 \mu\text{m}$ green line, $\Delta\delta = 0.25 \mu\text{m}$ red line respectively for $v = 10 \text{ m/s}$, $v = 15 \text{ m/s}$ and $v = 20 \text{ m/s}$). This shows that POD-FT allows one to deliver pulses with a spatial accuracy lower than $1 \mu\text{m}$, independently from v and up to $v = 20 \text{ m/s}$.

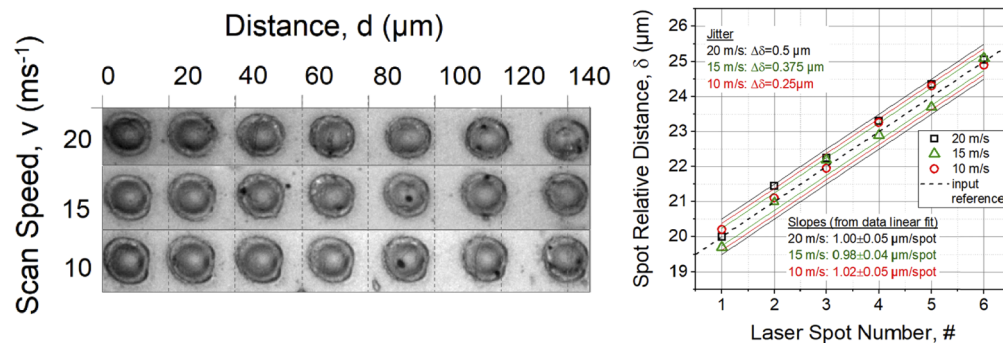


Fig. 2. Visual appearance of the laser spot impacts on PET (left). For all the v values, pulses were triggered with a temporal delay corresponding to a relative distance δ varying from $20 \mu\text{m}$ (left side) to $25 \mu\text{m}$ (right side) with an increment of $1 \mu\text{m}$. The graph (right side) shows the values of δ we measured via software versus the laser spot number for $v = 10 \text{ m/s}$ (red circle), $v = 15 \text{ m/s}$ (green triangles) and $v = 20 \text{ m/s}$ (black squares). Also plotted the ideal case (black dashed line) of δ increasing from impact to impact of $1 \mu\text{m}$ and the uncertainty induced by the jitter for $v = 10 \text{ m/s}$ (red lines) $v = 15 \text{ m/s}$ (green lines) and $v = 20 \text{ m/s}$ (black lines).

Figure 3 shows the visual appearance of laser impacts obtained in the same experimental conditions as Fig. 2 with the difference that Δt was adjusted to enable an increasing relative distance ($\delta = 10 \mu\text{m}$, $\delta = 20 \mu\text{m}$, $\delta = 30 \mu\text{m}$, $\delta = 50 \mu\text{m}$) in Fig. 3 top-left and decreasing in Fig. 3 top-right ($\delta = 50 \mu\text{m}$, $\delta = 30 \mu\text{m}$, $\delta = 10 \mu\text{m}$, $\delta = 5 \mu\text{m}$). We observe that since v is fixed, the first case corresponds to a decrease of the repetition rate whilst in the second the repetition rate increases. Importantly, not only are the impacts well positioned but the profile relative to a given

v value shows peaks with similar depth dz for the repetition rate increases and decreases (see respectively Fig. 3 bottom-left and bottom-right). We believe this demonstrates that the pulse energy doesn't change significantly when pulses are triggered on demand. This is also confirmed as the size of impacts does not change significantly from each other. In fact, for each v value, all the impacts are tangent to the dashed-point blue lines plotted in Fig. 3 which are parallel and are equally spaced.

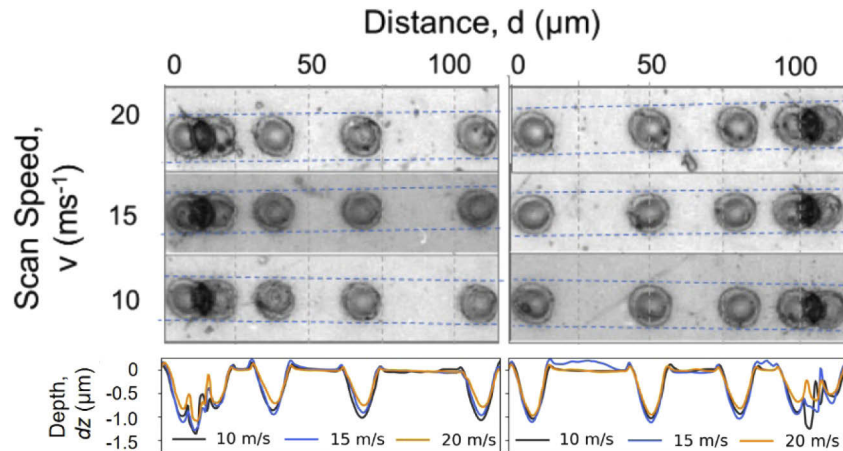


Fig. 3. Visual appearance of the laser spot impacts on PET. For all the v values, pulses were triggered with a temporal delay corresponding to a relative distance (from left to right) $\delta = 10 \mu\text{m}$, $\delta = 20 \mu\text{m}$, $\delta = 30 \mu\text{m}$, $\delta = 50 \mu\text{m}$ (left side) and $\delta = 50 \mu\text{m}$, $\delta = 30 \mu\text{m}$, $\delta = 20 \mu\text{m}$, $\delta = 10 \mu\text{m}$ (right side). Also shown the depth of the impacts for $v = 10 \text{ m/s}$ (black line) $v = 15 \text{ m/s}$ (blue line) and $v = 20 \text{ m/s}$ (orange line). Also plotted (blue dashed line) parallel lines which are tangent to each group of impacts.

3.2. Comparative evaluation of set-up performances

Figure 4 shows the up-right corners of the $5 \text{ cm} \times 5 \text{ cm}$ squares obtained after $N = 10$ passes with a scan speed $v = 2.5 \text{ m/s}$, $v = 10 \text{ m/s}$, $v = 15 \text{ m/s}$ and $v = 20 \text{ m/s}$. With respect to the section 3.1, a different software was used to control both scanner and laser (laserDESK). Moreover, the trigger signal generated was injected directly in the laser to control pulse emission. Three different scanning strategies were used, POD-FT (Fig. 4(a)), conventional (Fig. 4(b)) and SW (Fig. 4(c)).

Starting from $v = 2.5 \text{ m/s}$ we observe that for conventional scanning, pulses tend to overlap in the corners where the acceleration is higher (see Fig. 4(b)). The overlapping becomes more evident for higher values of v and pulses are undistinguishable over $v = 10 \text{ m/s}$.

A different behavior is observed for POD-FT and SW. In both cases pulses are kept well separated independently from the v values, this is highlighted at the corner edges. Nonetheless, from Fig. 4(a) it can be easily observed that when using POD-FT, still δ slightly varies in correspondence of the cornered edge where the galvo mirror acceleration is higher. There are a number of factors having an effect on the variation of δ when using POD-FT, we mention in particular the latency delay. Figure 5 shows the results we obtained after the « latency delay » has been taken into account in the calculation of the instant that the laser pulse is triggered by the scanner board (RTC6) combined with the software DMC + XL SCAN. It can be observed that pulses are now equally spaced independently from both the scan speed (from $v = 7.5 \text{ m/s}$ to $v = 20 \text{ m/s}$ with a step of $v = 2.5 \text{ m/s}$) and the acceleration value. No spot accumulation is observed in the corners. We can therefore conclude that after the latency delay has been compensated the

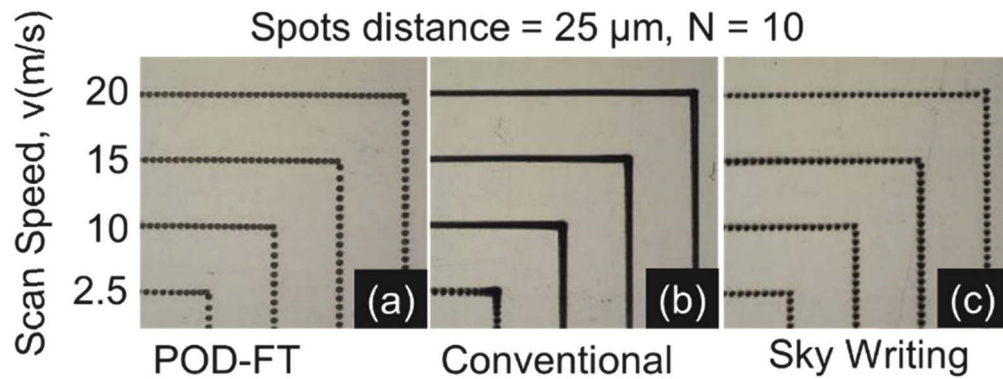


Fig. 4. The figure shows the up-right corners relative to three sets of squares obtained (a) with POD-FT, (b) with conventional scanning, (c) with SW. Each set is composed of four squares corresponding to 4 different v values $v = 2.5$ m/s, $v = 10$ m/s, $v = 15$ m/s and $v = 20$ m/s. In all cases the number of laser passes is $N = 10$ and the distance between the pulses has been fixed to $\delta = 25$ μm .

POD-FT enables an excellent pulse to pulse control which is not only < 1 μm (see Fig. 2(b)) but is also comparable to the SW approach.

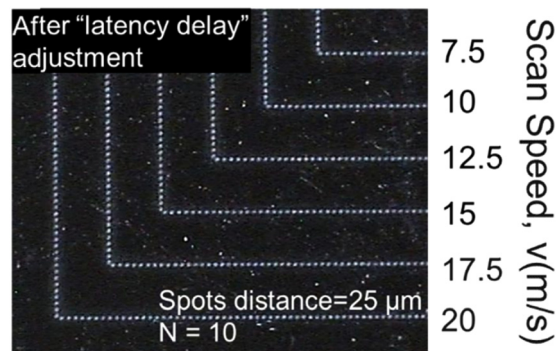


Fig. 5. The figure shows a set of 6 squares obtained with POD-FT scanning, $N = 10$ repetitions and scan speed varying from $v = 7.5$ m/s to $v = 20$ m/s. In all cases the spot distance was fixed to $\delta = 25$ μm and the latency delay has been taken into account by the scanner board when triggering pulses.

3.3. Highly precise engraving

Figure 6 shows a part of the letter “A” that was engraved following three different approaches POD-FT, Conventional Scanning and SW. During the tests we varied the scan speed ($v = 0.9$ m/s, $v = 3.6$ m/s and $v = 7.2$ m/s) and the repetition rate (respectively $f = 100$ kHz, $f = 400$ kHz and $f = 800$ kHz) in order to keep δ unchanged ($\delta = 9$ μm which correspond to an overlap of 40%). It is worth observing that in the case of POD FT the f value is only a reference value that can varies pulse by pulse following the scanner “demand. The number of scans N was fixed to $N = 75$ (see experimental part) as well as the pulse energy $E = 4\mu\text{J}$ and the hatch = $3\mu\text{m}$. Starting from $v = 0.9$ m/s et $f = 100$ kHz we obtained similar results in terms of machining quality with similar depth and flat bottom. With $v = 3.6$ m/s, $f = 400$ kHz for conventional scanning, a degradation of the machining quality is observed. In particular, important phenomena of over-engraving induced on

the bottom groove contour by the galvo mirror acceleration are now visible (see black contour in Fig. 6(e)) No remarkable variations are observed for POD-FT and SW. Finally, when $v = 7.2$ m/s slight over-engraving is observed also in the case of POD-FT and SW (see deep blue part in 3D profiles of Fig. 7) but in the case of conventional scanning this phenomenon becomes dramatic with a deep over engraving in the correspondence of the groove contour. As shown in Fig. 7 (yellowish part of Fig. 7 middle), the profilometer is even unable to measure the depth of the over-engraved part. We believe this is due to its high aspect ratio which induce a lack of reflected light.

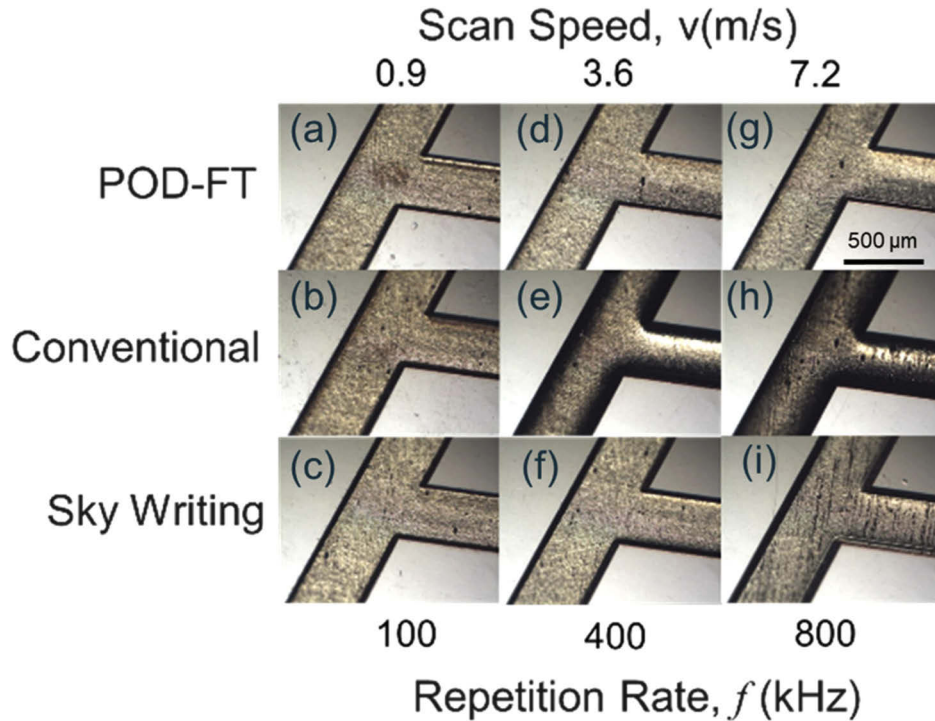


Fig. 6. The figure shows a part of a letter “A” engraved by laser utilising three scanning approach POT-FT (top row), Conventional (middle row) and SW (bottom row). For each scanning approach we varied the scan speed $v = 0.9$ m/s (left column) $v = 3.6$ m/s (central column) $v = 7.2$ m/s (right column). In order to keep the distance between pulses $\delta = 9 \mu\text{m}$ unchanged, when varying v , we proportionally varied the repetition rate $f = 100$ kHz, $f = 400$ kHz, $f = 800$ kHz. The number of scans was fixed to $N = 75$.

These results are confirmed by SEM analysis shown in Fig. 8.

We can therefore conclude that increasing v from 0.9 m/s to 7.2 m/s will induce severe over engraving in the groove bottom-sides due to the increase of overlapping which in turn is induced by the galvo acceleration. This phenomenon is strongly reduced by adopting different scanning approaches like POD- FT or SW. Furthermore, with $v = 7.2$ m/s the time to accomplish the $N = 75$ scans is $t = 167$ s for POD-FT leading to an ablation efficiency of roughly $\alpha_{\text{FT}} \approx 0.011 \text{ mm}^3 \cdot \text{min}^{-1} \cdot \text{W}^{-1}$ and becomes $t = 276$ s for SW corresponding to $\alpha_{\text{SW}} \approx 0.0063 \text{ mm}^3 \cdot \text{min}^{-1} \cdot \text{W}^{-1}$. Both are compatible with data previously reported in literature for the same fluence value ($\Phi = 2.26 \text{ J} \cdot \text{cm}^{-2}$) and multi-pass processing [6]. Thus, although POD-FT and SW are both valid alternatives for a precise engraving, POD-FT respect to SW enables a reduction of the scanning time by nearly 40% which contribute to sensibly boost the process throughput.

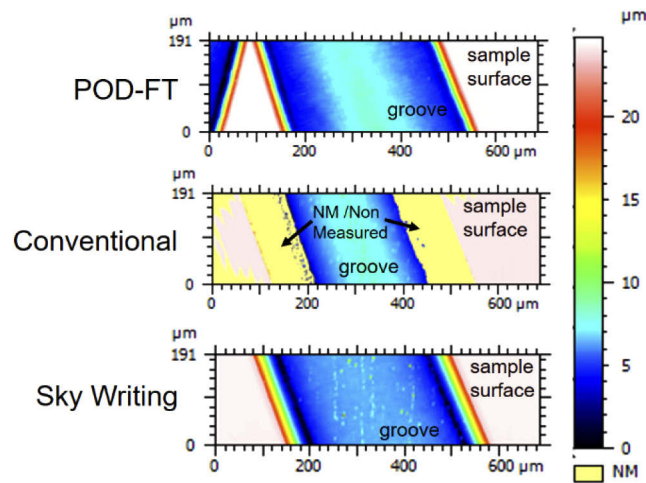


Fig. 7. 3D profiles of the engraved part (groove) in the case of $v = 7.2$ m/s and $f = 800$ kHz for three scanning approaches: POD-FT (up), conventional (middle) and Sky Writing (bottom). In the case of Conventional scanning (middle) the profilometer was unable to measure the contour of the groove (see NM, yellowish, part).

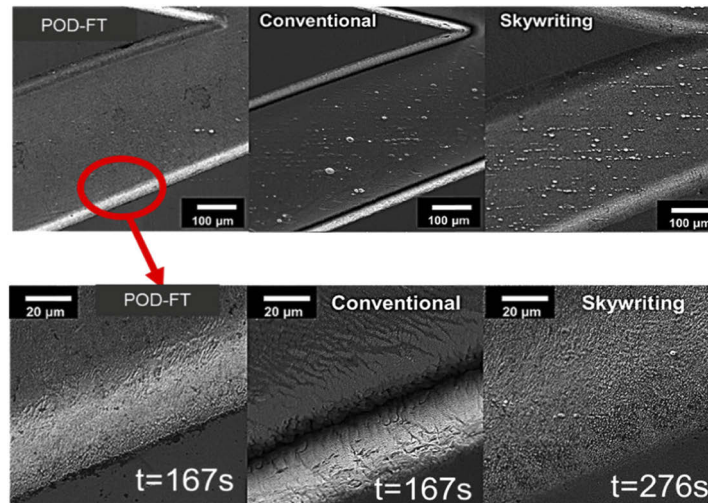


Fig. 8. SEM micrographs of the “A” engraved by laser using three scanning approach: POD-FT (left), Conventional (middle) Sky Writing (right). The scan speed was $v = 7.2$ m/s and the repetition rate 800 kHz. Also shown (bottom row) a particular of the groove contour and the processing time.

4. Conclusion

An innovative POD scanning technique for high repetition rate, industrial, femtosecond laser sources has been introduced and tested based on two recent innovative technologies. The first is a mode locked CPA femtosecond laser which can deliver pulses on demand and with flexible repetition rates combined with constant pulse energies. The second is a galvo scanner and control board (excelliSCAN 14 with RTC6), which can calculate and predict the exact time to trigger pulse emission by taking into account the acceleration of the galvo mirrors. A clear

advantage of this approach has been shown in respect to conventional scanning with a fixed repetition rate by increasing the pulse to pulse position control tackling issues coming from pulse accumulation. It has been shown that pulses can be delivered with 1 μm accuracy at scan speed as high as 20 m/s and that the pulse energy doesn't change substantially when adapting the repetition rate to the pulse demand. In terms of accuracy, the proposed approach shows performances comparable to well established technologies like SW. Moreover, for applications like engraving where several passes and direction changes are required, POD-FT shows the advantage of reducing the processing time (up to 40% in the case reported) since no extra galvo movements are required to manage acceleration. We believe that a wide variety of applications like laser scribing, highly precise patterning, surface structuring, drilling of precise micro holes matrix, etc. will benefit from the POD-FT both in term of precision and throughput, thus paving the way for an ever more ubiquitous use of ultrashort pulse laser technology in industrial environments like micro- and consumable electronic, micro-mechanic, etc.

Acknowledgments

This paper has been supported by Nouvelle Aquitaine Region in the framework of "TrulyFast" project.

Disclosures

The authors declare no conflicts of interest

References

1. A. Y. Vorobyev and C. Guo, "Direct creation of black silicon using femtosecond laser pulses," *Appl. Surf. Sci.* **257**(16), 7291–7294 (2011).
2. M. Bieda, M. Siebold, and A. F. Lasagni, "Fabrication of sub-micron surface structures on copper, stainless steel and titanium using picosecond laser interference patterning," *Appl. Surf. Sci.* **387**, 175–182 (2016).
3. J. Bonse, S. Höhm, S. V. Kirner, A. Rosenfeld, and J. Krüger, "Laser-Induced Periodic Surface Structures— A Scientific Evergreen," *IEEE J. Sel. Top. Quantum Electron.* **23**(3), 9000615 (2017).
4. R. Osellame, S. Taccheo, M. Marangoni, R. Ramponi, P. Laporta, D. Polli, S. De Silvestri, and G. Cerullo, "Femtosecond writing of active optical waveguides with astigmatically shaped beams," *J. Opt. Soc. Am. B* **20**(7), 1559–1567 (2003).
5. G. Kamlage, T. Bauer, A. Ostendorf, and B. N. Chichkov, "Deep drilling of metals by femtosecond laser pulses," *Appl. Phys. A: Mater. Sci. Process.* **77**(2), 307–310 (2003).
6. John Lopez, Konstantin Mishchik, Girolamo Mincuzzi, Eric Audouard, Eric Mottay, and Rainer Kling, "Efficient metal processing using high average power ultrafast laser," *J. Laser Micro/Nanoeng.* **12**(3), 296–303 (2017).
7. Seongkuk Lee, Dongfang Yang, and Suwas Nikumb, "Femtosecond laser micro-milling of Si wafers," *Appl. Surf. Sci.* **254**(10), 2996–3005 (2008).
8. <https://amplitude-laser.com/produit/tangor/> Amplitude Système web site retrieved in data 14/02/2020
9. <https://www.amphos.de/products/> Amphos GmbH web site, retrieved in data 14/02/2020
10. <https://www.afs-jena.de/> Activefiber web site, retrieved in data 14/02/2020
11. T. Mans, J. Dolkemeyer, and C. Schnitzler, "High Power Femtosecond Lasers," *Laser Tech. J.* **11**(3), 40–43 (2014).
12. E. Shestae, D. Hoff, A. M. Saylor, A. Klenke, S. Hädrich, F. Just, T. Eidam, P. Jójárt, Z. Várallyay, K. Osvay, G. G. Paulus, A. Tünnermann, and J. Limpert, "High-power ytterbium-doped fiber laser delivering few-cycle, carrier-envelope phase-stable 100 μJ pulses at 100 kHz," *Opt. Lett.* **45**(1), 97 (2020).
13. C. G. E. Alfieri, A. Diebold, F. Emaury, E. Gini, C. J. Saraceno, and U. Keller, "Improved SESAMs for femtosecond pulse generation approaching the kW average power regime," *Opt. Express* **24**(24), 27587–27599 (2016).
14. M. Müller, M. Kienel, A. Klenke, T. Gottschall, E. Shestae, M. Plötner, J. Limpert, and A. Tünnermann, "1 kW 1 mJ eight-channel ultrafast fiber laser," *Opt. Lett.* **41**(15), 3439–3442 (2016).
15. S. Faas, R. Weber, and T. Graf, "Heat accumulation-controlled surface functionalization of stainless steel with structuring rates up to 500 mm²/s," *Procedia CIRP* **74**, 324–327 (2018).
16. F. Bauer, A. Michalowski, T. Kiedrowski, and S. Nolte, "Heat accumulation in ultra-short pulsed scanning laser ablation of metals," *Opt. Express* **23**(2), 1035–1043 (2015).
17. T. Kramer, S. Remund, M. Chaja, M. Gafner, T. Maehne, and B. Neuenschwander, "High Throughput and High Quality Surface Texturing with Ultrafast Lasers," in Laser Congress 2019 (ASSL, LAC, LS&C), OSA Technical Digest (Optical Society of America, 2019), paper CW1C.5. Doi: <https://doi.org/10.1364/LAC.2019.CW1C.5>
18. G. Mincuzzi, A. Rebière, J. Lopez, M. Faucon, and R. Kling, "New fast galvo scanner head for high throughput micromachining," *Proc. SPIE* **10520**, 105200X (2018).

19. B. Jaeggi, B. Neuenschwander, M. Zimmermann, L. Penning, R. deLoor, K. Weingarten, and A. Oehler, "High-throughput and high-precision laser micromachining with ps-pulses in synchronized mode with a fast polygon line scanner," *Proc. SPIE* **8967**, 89670Q (2014).
20. G. Mincuzzi, A. Rebière, B. Le Goaec, S. Nourry, P. Pagano, M. Faucon, and R. Kling, "Beam engineering for high throughput material processing with high power, femtosecond lasers," *Proc. SPIE* **10906**, 109061B (2019).
21. G. Mincuzzi « Beam engineering for high throughput material processing », PLI Conference, Colmar (France) 2019, 25 and 26 September 2019
22. R. De Loor, "Polygon Scanner System for Ultra Short Pulsed Laser Micro-Machining Applications," *Phys. Procedia* **41**, 544–551 (2013).
23. A. Owyong, G. R. Hadley, P. Esherick, R. L. Schmitt, and L. A. Rahn, "Gain switching of a monolithic single-frequency laser-diode-excited Nd:YAG laser," *Opt. Lett.* **10**(10), 484–486 (1985).
24. J. A. Morris and C. R. Pollock, "Passive Q switching of a diode-pumped Nd:YAG laser with a saturable absorber," *Opt. Lett.* **15**(8), 440–442 (1990).
25. Vid Agrež and Rok Petkovšek, "Highly adaptable gain-switched fiber laser with improved efficiency," *Opt. Express* **27**(9), 12100–12109 (2019).
26. F. Basin, J. Pouysegur, M. Delaigue, B. Trophème, J. Sanabria, E. Mottay, and C. Hönninger, ">300-W femtosecond laser with free triggering up to 25 MHz," in *Conference on Lasers and Electro-Optics*, OSA Technical Digest (Optical Society of America, 2019), paper ATu4I.5. Doi: https://doi.org/10.1364/CLEO_AT.2019.ATu4I.5
27. C. Hönninger and E. Audouard, "Multi 100 W Femtosecond Laser Perspectives," *Laser Tech. J.* **15**(2), 50–53 (2018).